


Prospect of using Grover's search in the noisy-intermediate-scale quantum-computer eraYulun Wang  and Predrag S. Krstic **Institute for Advanced Computational Science, Stony Brook University, Stony Brook, New York 11794-5250, USA* (Received 21 June 2020; accepted 18 September 2020; published 20 October 2020)

In order to understand the bounds of utilization of Grover's search algorithm for large unstructured data in the presence of quantum computer noise, we undertake a series of simulations by inflicting various types of noise, modeled by the IBM QISKIT. We apply three forms of Grover's algorithm: (i) the standard one, with 4–10 qubits; (ii) a recently published modified Grover's algorithm, set to reduce the circuit depth; and (iii) the algorithms in (i) and (ii) with multicontrol Toffoli's gates modified by the addition of an ancilla qubit. Based on these simulations, we find the upper bound of noise for these cases, establish its dependence on the quantum depth of the circuit, and provide comparison among them. By extrapolation of the fitted thresholds, we predict what would be the typical gate error bounds when applying Grover's algorithms for the search of data in a data set as large as 32 000.

DOI: [10.1103/PhysRevA.102.042609](https://doi.org/10.1103/PhysRevA.102.042609)**I. INTRODUCTION**

Grover's algorithm (GA) [1,2] for the search of unstructured data shows an obvious and convincing quantum advantage to the classical search algorithms. Thus, GA scales the number of search iterations (i.e., the search time) with \sqrt{N} rather than with N in the classical search, where N is the number of searched data. This polynomial acceleration has been proved to be optimal for the data search problems [3]: A search job that would run on a classical computer one month would take about 3.5 h to finish on a quantum computer using Grover's algorithm.

Running algorithms such as Grover's search on modern, quantum-circuit-based quantum computers is achieved by consecutive unitary operations. However, the imperfect quantum gates and the thermally induced decoherence in the NISQ (noisy intermediate-scale quantum) computers are the major source of noise in current hardware, producing errors in the quantum operations [4]. The size of the quantum circuit is characterized by the total number of gates, and often by the circuit depth, the largest number of gates along any input-output path, moving forward in time. Thus, circuit depth is proportional to the smallest amount of time steps to execute the circuit, assuming that each gate is performed within a time step, and the gates that act on independent qubits can be executed simultaneously. Many researchers have analyzed the impact of various noise types in Grover's search algorithm [5–9]. With a large circuit depth, quantum programs for complex tasks propagate and accumulate errors throughout the whole quantum circuit. As a consequence, the search for the targeted data fails because of the small signal-to-noise ratio. For example, with the current level of noise in superconducting quantum devices (like the IBM Q and Rigetti), one could clearly select an element among 8 data (3 qubits),

while the search for an element among the 16 data (4 qubits) fails. We show in Fig. 1 the results of the search of the 0011 element at the 4-qubit Hilbert space using an IBM Q computer of the latest generation. Due to the noise the targeted state probability is not distinguishable from the probabilities of the other states. A deterministic version of GA [10] has been proposed to keep the ideal target probability 100% for any size of database, which is slightly improved from the standard GA (SGA) [1], but it does not necessarily help to distinguish a searched target in the presence of the noise. For the SGA, the circuit depth and the total number of gates exponentially increase with the number of qubits, which might induce exponential magnification of the noise assuming the worst case that errors are produced with some probability at each gate. For example, the circuit depth with 3 qubits is 58 (95 gates), with 4 qubits the depth grows to 242 (322 gates), and for 6 qubits it reaches 1922 (2418 gates).

In this work we define the selectivity S ,

$$S = 10 \log_{10} (P_t/P_{\text{hn}}), \quad (1)$$

to be the metric that quantifies the performance of the quantum algorithm, where P_t is the measured probability of the targeted state and P_{hn} is the probability of the highest measured noise signal. The selectivity decreases with increases of the noise probabilities. In Fig. 1, the largest noise-induced probability is of the 0000 state (7.6%), which is higher than the target probability (6.6%), leading to a negative selectivity, indicating an unsuccessful search. In this study we choose $S = 3$ for the lowest acceptable threshold of the selectivity, which corresponds to $P_t/P_{\text{hn}} \approx 2$. When $S = 3$ is reached, the item searched by Grover's algorithm is considered well distinguishable from the noise, and we consider the algorithm to be successfully executed. Thus, this value of the selectivity defines the highest acceptable bound of the noise for the successful Grover's operation. The threshold error probabilities and damping parameters in this work are obtained by interpolating the computed data to the selectivity $S = 3$.

*krsticps@gmail.com

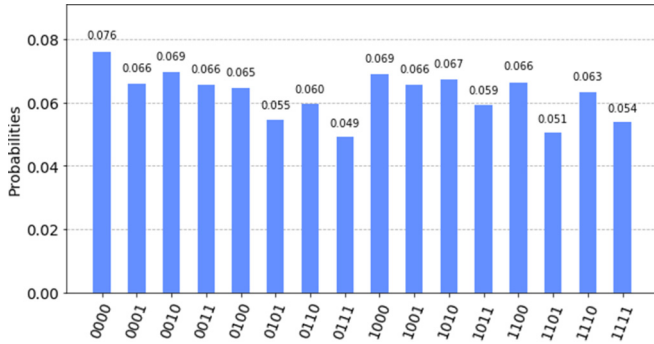


FIG. 1. The 4-qubit Grover's search of 0011 in a set of 16 data on IBM's latest quantum computer "ibmq_paris." The ideal probability to measure "0011" is 96.7%; however, the measured one is only 6.6% due to the quantum noise and the specific topology of the machine.

The goal of this paper is not to mitigate the errors in Grover's quantum circuit, but rather to predict how small these errors need to be in order to reach the acceptable selectivity of the targeted state. This is done by replicating various types of noise in the circuits and performing simulation of Grover's algorithm by varying the number of qubits n from 4 to 10, which alters the size of the searched data sets as 2^n . The quantum circuit depth is increased exponentially with the number of qubits using the SGA reflecting the dependence on n of the multicontrol Toffoli (MCT) gates present in oracle and diffusion operators as well as the number of iterations, proportional to $2^{n/2}$ (see Note SI in the Supplemental Material [11]). However, this increase can be restrained by adding ancillas to MCTs (labeled here as MCTA) in both the SGA and the recently published Grover's algorithms modified (MGA) for reduction of the circuit depth [12]. With fewer gates in a circuit, smaller gate operational errors are accumulated, and the coherent time domain is increased. We find that adding one ancilla to the MCTs, as done in IBM Quantum Information Science Kit (QISKIT) [13] following Barenco *et al.* [14], strongly reduces the circuit depth and consequently reduces the overall noise in all studied cases.

In Sec. II we introduced the background of noise simulation, as defined in QISKIT. In Secs. III and IV we perform experiments of simulation for various errors by varying the number of qubits (i.e., varying the number of gates in the quantum circuit) to obtain the upper bound of the thresholds toward a successful Grover's search. The SGA with the use of MCTs and MCTAs is studied in Sec. III for the circuit depth and the response to the various errors in the circuit. The same is done in Sec. IV where the error response of the modified GA, which achieves circuit depth reduction by use of the local diffusion operators [12], is studied. In Sec. V we provide comparison of the selectivity thresholds due to the errors between all considered algorithms, highlighting the most successful ones. Finally, in Sec. VI we give our conclusions.

II. NOISE SIMULATION

Various types of errors have been identified and characterized in superconducting quantum computers. The design of a quantum computer can be evaluated by the coherence time of a qubit (natural relaxation time, T_1 , and the time for the

qubit dephasing from the superposition state, T_2), as well as by the gate errors [single-qubit rotations and 2-qubit operations, such as controlled-NOT (CNOT)] [15] and readout errors. Soft methods have been developed to mitigate particular error types. However, the utilization of these methods makes the quantum circuit more complex, bringing in more gates and more errors, which limits their effectiveness.

In the real quantum devices, qubits suffer simultaneously from various types of gate errors and decoherence, which makes extraction of the effects of the individual errors a formidable task. The error probabilities are often characterized by the qubit multiplicity of the various quantum operations. For the latest superconducting quantum-computers from IBM (for example, ibmq_cambridge at 18:23:30 on May 4, 2020), single qubit instructions have an average error probability of 0.093% for U_2 gate operations and 0.19% for U_3 gate operations, while the CNOT gates have an average error probability of 3.5%. The U_3 gate is defined in QISKIT as a single-qubit rotation gate with three Euler angles: θ , ϕ , and λ by $U_3(\theta, \phi, \lambda) = R_Z(\phi)R_X(-\frac{\pi}{2})R_Z(\theta)R_X(\frac{\pi}{2})R_X(\lambda)$, where $R_Z(\theta)$ and $R_X(\theta)$ are the single-qubit rotations around the Z and X axes with an angle of θ on the Bloch sphere, while the U_2 gate is defined as $U_2(\phi, \lambda) = U_3(\frac{\pi}{2}, \phi, \lambda)$. Besides gate errors, this machine also suffers from a significant readout error at average 9.5% and limited coherent time (average $T_1 = 82 \mu\text{s}$ and $T_2 = 41 \mu\text{s}$).

We study the effects of the gate and the coherent qubit time errors as modeled in QISKIT (version 1.16.0) [13]. Gate errors such as bit and phase flip (so-called Pauli errors) and depolarization are modeled by assuming that an error happens with some probability in each gate in the quantum circuit [16]. The Kraus operators for the Pauli errors are defined in QISKIT as $E_0 = \sqrt{1-p_\sigma}I$ and $E_1 = \sqrt{p_\sigma}\sigma$, where p_σ is the error probability and $\sigma = X$ (bit flip), Z (phase flip), Y (combined flips), respectively [13]. These operators yield the mixed states $\rho' = \varepsilon(\rho) = E_0\rho E_0^\dagger + E_1\rho E_1^\dagger = (1-p_\sigma)\rho + p_\sigma\sigma\rho\sigma$, where the initial state is described by the density operator ρ and the functional ε is the quantum operation. A qubit is flipped with probability p_σ or left unchanged with probability $1-p_\sigma$. With a depolarization error, a qubit is depolarized with a probability p_{dep} . The depolarization channel is defined as $\varepsilon(\rho) = (1-p_{\text{dep}})\rho + p_{\text{dep}}\frac{I}{2^n}$, where I is the completely mixed state density and n is the number of qubits in the error channel [17].

Keeping a quantum state coherent is essential for implementation of gate operations and measurements of qubits in quantum computing. Induced by external disturbances, decoherence erodes the fidelity of quantum executions due to coupling between the quantum system and the environment. Thus, decoherence of quantum states is a large obstacle to scalable quantum computing. We study the Grover's circuit response to the amplitude damping (AD) and the phase damping (PD). In these cases the dimensionless damping probability p_{dam} defines the Kraus operators $E_{0,1}$ [17,18] as $E_0|0\rangle = |0\rangle$, $E_0|1\rangle = \sqrt{1-p_{\text{dam}}}|1\rangle$, and $E_1|0\rangle = 0$ for both AD and PD, while $E_1|1\rangle = \sqrt{p_{\text{dam}}}|x\rangle$, where $x = 0$ for AD and $x = 1$ for PD, p_{dam} is the probability of either energy loss (AD) or information loss (PD) to the environment in a small time interval δt . After these dissipation processes repeat many (m) times in succession, during the gate time $t_g = m\delta t$, the

corresponding transition channel decays exponentially [19] as $e^{-\Gamma t_g}$, where Γ is the probability rate $\Gamma = \frac{P_{\text{dam}}}{\delta t}$. The amplitude damping is often referred to as the relaxation process for the time T_1 , where $T_1 = \frac{1}{\Gamma}$ and Γ is the amplitude-damping probability rate. Similarly, the phase damping is referred to as the superposition dephasing process for the time T_2 , where $T_2 = \frac{1}{\Gamma}$ and Γ is the phase-damping rate. T_1 and T_2 together are employed to characterize the lifetime of the qubit's amplitude and phase. The quantum error channels mentioned above are applied to all single-qubit quantum operations during the noise simulation. The error channels for 2-qubit operations are obtained by applying the single-qubit error to each of two qubits (for example, CNOT) [13].

QISKIT supports simulation of the thermal relaxation mode by inputting values for T_1 and T_2 with predefined gate time t_g , where $T_2 \leq 2T_1$ [20,21]. The gate time t_g in the model is set to 50 ns for single-qubit U_2 rotations, 100 ns for U_3 rotations, 300 ns for CNOT gates, 1000 ns for qubit reset, and 1000 ns for measurements. The T_1 and T_2 relaxation error rates are defined as $\varepsilon_{T_1} = e^{-t_g/T_1}$ and $\varepsilon_{T_2} = e^{-t_g/T_2}$, respectively [22].

We also apply our error analysis of Grover's algorithm (with MCTs or MCTAs) to the method targeted to lowering the circuit depth (and fewer number of gates), recently published by Zhang and Korepin [12]. They achieved reduction of the number of gates by replacing the standard Grover's operator with the depth-modified one in adjusted sequences, in which the standard diffusion operator is replaced by a local diffusion operator [23]. Furthermore, the depth-reduced algorithm can be executed in multiple stages to eliminate noise. For example, the search target can be divided into two stages, t_1 and t_2 , with $|t_1\rangle = |t_2\rangle > |t_1\rangle$. After the first stage $|t_1\rangle$, partial measurement is applied to terminate the search in some of the qubits. The quantum measurements in the first stage can avoid qubit idling with unwanted noise in the second stage. The rest of the qubits are reset and reinitialized before the execution of the second stage, which also eliminates the unwanted noise accumulated in the first stage. We here apply MCTA gates of this modified Grover's algorithm, obtaining further reduction of the circuit depth and thus increasing the thresholds in all studied quantum errors.

III. GROVER'S CIRCUIT WITH ANCILLARY QUBITS

MCT gates are the key components of oracle and diffusion operators for the Grover's search. Current IBM quantum computers allow only elementary executions such as single-qubit rotations and controlled 2-qubit gates. Thus, the multiple-qubit Toffoli gates are decomposed to elementary operations during circuit transpiling by QISKIT and hence occupy the biggest part of the circuit depth, resulting in the main sources of noise. By using MCTAs the circuit depth and the number of total gates can be dramatically reduced. In this work, nonancilla Toffoli gates and 1-ancilla Toffoli gates are used for composing circuits with different depths. Circuits for the MCT and MCTA gates are generated by QISKIT functions (using `qiskit.aqua.circuits.gates.mct` with modes "noancilla" and "advanced" which are based on the gray-code sequence and the recursive splitting method for nonancilla and 1-ancilla Toffoli gates, respectively [14]). When designing quantum circuits, various searched targets have their unique oracles.

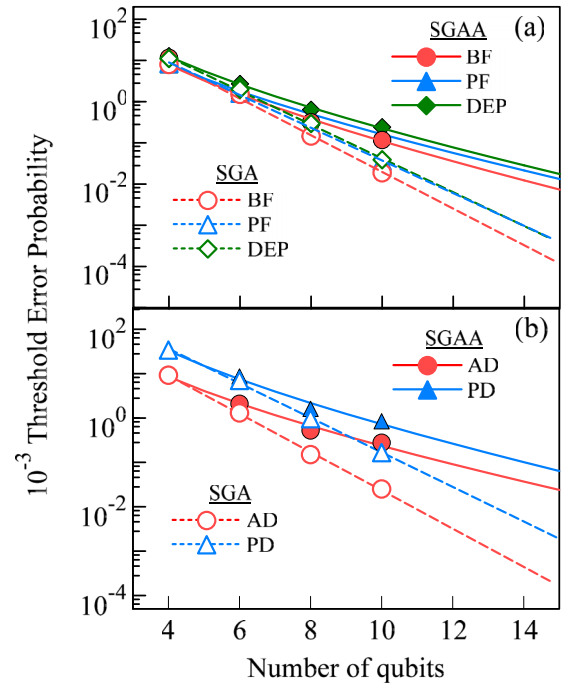


FIG. 2. Threshold error probabilities for (a) bit flip (BF), phase flip (PF), and depolarizing (DEP) and for (b) threshold damping parameters of amplitude damping (AD) and phase damping (PD), with various numbers of qubits in the GA search. The hollow symbols and solid symbols are for SGA and SGAA, respectively. Dashed (SGA) and solid (SGAA) lines are fitting curves with extrapolation, as described in the text.

Only one MCT gate is required to construct the oracle for the encoded search state $|1\rangle$. Hence for the simplest circuit, $|1\rangle^{\otimes n}$ is chosen as the searched target item in all tests [24]. The gate numbers and the circuit depth are calculated with QISKIT functions by varying the number of qubits from 4 to 14, for the SGA as well as for the circuits where MCTAs replaced MCTs (SGAA). These are shown in Table SI of the Supplemental Material [11]. For example, in the $n = 4$ qubit SGA, 3 iterations (marked as G_4^3) are applied, which yields 322 for the total number of gates. When using MCTAs, the reduction of the number of gates for $n = 4$ qubits is about 1.3 reduction. In the 10-qubit algorithm, the number of gates in the circuit is reduced nearly 10 times by using MCTAs. For the 14-qubit algorithm this reduction is nearly 50. This leads to a noticeable degradation of noise, especially when increasing the number of qubits, as our results below show.

We calculated the upper bounds of noise defined by the lowest acceptable selectivity defined in the Introduction. We present these bounds in Fig. 2 for both the SGA and the SGAA, by changing the types of noise and varying the number of qubits from 4 to 10. As discussed in the Introduction, using MCTAs in the SGA increases the upper bound of thresholds in all studied cases as a consequence of significant contraction of the quantum depths and the total number of gates (see Table SI in the Supplemental Material [11]). This contraction increases with the number of qubits. Even though the gate errors are accumulated after each gate operation, the noise is significantly suppressed with the reduction of the number

of gates. From Fig. 2, the circuit for the 4-qubit SGA requires the Pauli, depolarization, and amplitude-damping error probabilities below 10^{-2} and phase damping below 3×10^{-2} for acceptable search results, with similar conclusions for the SGAA. With the 8-qubit search, the SGA and the SGAA start deviating from each other. The 10-qubit SGA circuit requires error probabilities below 10^{-5} (except for phase damping $<10^{-4}$), while a circuit depth of the SGAA an order of magnitude lower than that of the SGA produces a leap in selectivity; i.e., error thresholds are of the order of 10^{-4} . Thus, when searching a database of the size of 2^{10} , the upper bound of the depolarization error, for example, is about 2×10^{-4} . Similar conclusions can be obtained for amplitude-damping ($<2 \times 10^{-4}$) and phase-damping ($<7 \times 10^{-4}$) noise, as well as for bit-flip and phase-flip error probabilities ($<10^{-4}$): the threshold parameter values increase an order of magnitude in 10-qubit cases when MCTAs are used.

The selectivity thresholds in Fig. 2 are directly correlated to the number of gates in the circuits when varying the number of qubits. To understand this correlation, we first fitted the data for the number of gates in Table SI of Supplemental Material [11] vs the number of qubits (4 to 14 qubits) using the functional forms inspired by the analysis of Barenco *et al.* [14] on the number of gates in the MCTs with and without ancilla. This is explained in detail in Note SI of the Supplemental Material [11]. For the SGA case, the number of gates (G) is an exponential function of n , with the fitting function $G_{\text{SGA}} = 4.6991e^{1.0388n}$, reflecting the number of iterations, $2^{n/2}$, as well as 2^n functional dependence of MCTs on n . However, the combined product of exponential and power dependencies fits best the SGAA cases, $G_{\text{SGAA}} = 1.2761n^{2.8401}e^{0.3436n}$. The exponent here corresponds to the $2^{n/2}$ number of iterations, which confirms the polynomial dependence of the number of gates on a MCT with ancilla [14]. Similar functional dependencies are obtained for the circuit depths of the SGA and the SGAA, due to the almost constant ratio of number of gates and the circuit depth in Table SI of the Supplemental Material [11]. Since it is expected that the quantum errors are accumulated proportionally to the number of gates in a circuit, it is not surprising that the best fits for the selectivity thresholds (lines in Fig. 2) are obtained with fitting models similar to those for G_{SGA} and G_{SGAA} , even with similar values of exponents. The fitted curves, obtained with high correlations, are shown in Fig. 2 with dashed and solid lines and fitting parameters are listed in Table SII of the Supplemental Material [11]. Although the simulations were done with a top-of-the-line supercomputing cluster [25], 10 qubits was the limit for successful simulation of GA with QISKIT, mainly due to the large memory requirements in a classical computer. Still, by extrapolation of the obtained fits we can predict with certainty the selectivity thresholds for larger numbers of qubits. Thus, for the SGA with 15 qubits the threshold error probabilities are as low as 10^{-6} for phase damping and 10^{-7} for other types of errors. However, the SGAA improves the error threshold by about 2 orders of magnitude. For example, the upper bound of depolarizing noise increases from about 4×10^{-7} to 1.75×10^{-5} .

Calculated variations of the thermal relaxation times T_1 and T_2 with the number of qubits are presented in Fig. 3. Symbols in the figure show thresholds of the lower bound for T_1 and T_2

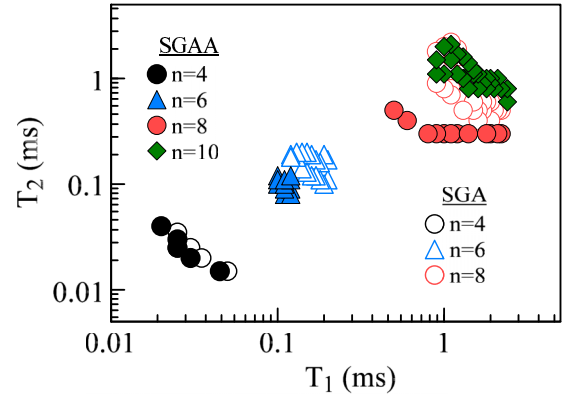


FIG. 3. Selectivity thresholds for the thermal relaxation times of the SGA and the SGAA with various numbers of qubits.

defined for the selectivity in the range 2.5 to 3.5 (i.e., P_t/P_{hn} in range 1.778 to 2.239). Unlike the other types of noise where it was favorable to have a bigger threshold, T_1 and T_2 are desired to have lower thresholds, which leads to a smaller coherent time for execution of the SGA and the SGAA. Each point in the figure is independently calculated and collected for given T_1 and T_2 . The results for the 10-qubit SGA search could not be obtained because the thresholds T_1 and T_2 exceed the QISKIT simulation limits ($2500 \mu\text{s}$). For example, a successful search through a set of 2^4 data can be done with T_1 and T_2 in the range of 15–50 μs with both the SGA and the SGAA, which is well achievable by current quantum hardware. For the 2^6 data set, the thresholds for T_1 and T_2 increase to about 100 μs with the SGAA and close to 200 μs with the SGA, while for the 8-qubit search T_1 and T_2 average around 1150 and 330 μs , respectively, with the SGAA, but about 1230 and 590 μs , respectively, with the SGA. For the 10-qubit SGA, the requirements for T_1 and T_2 exceed 10 ms with a total circuit depth of 128 002. Better results are obtained with the SGAA. Thus, the relaxation time limits for T_1 and T_2 with 10 qubits average 1.8 and 1 ms, respectively.

IV. GROVER'S CIRCUIT BY LOCAL DIFFUSION OPERATORS

The selectivity thresholds are calculated in this section for the GA with a modified circuit to reduce the quantum depth [12] (MGA) in two variants, one-stage (M1GA) and two-stage (M2GA) with inclusion of noise, as was done in Sec. III. In addition, we also studied the MGA with one ancilla in MCTs (MkGAA, $k = 1$ and 2), which showed, like in the case of the SGAA, a further improvement in the error thresholds. Table SIII in the Supplemental Material [11] contains the studied configurations as well as the information on the relevant quantum depths and the number of gates (including both 1- and 2-qubit gates). One-stage and two-stage methods of depth optimization are both tested for 4–10 qubit cases. Figure S2 in Note SII of the Supplemental Material [11] illustrates schematically, as an example, the quantum circuits for the SGA and the MGA configurations with 4 qubits. The MGA circuit configurations in Table SIII of the Supplemental Material [11] are also studied using MCTAs in place of MCTs, convincingly reducing the depth of the circuits.

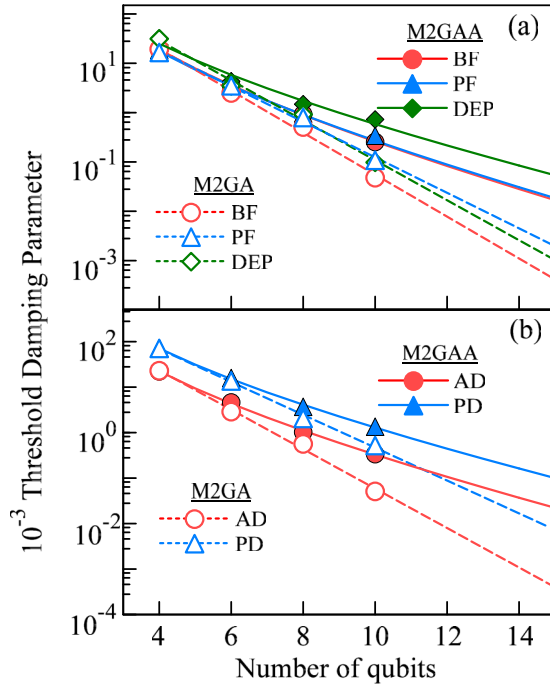


FIG. 4. Fitting curve of selectivity thresholds for the error probability vs the number of qubits for various types of errors [BF, PF, and DEP in panel (a) and AD and PD in panel (b)] applied at the two-stage depth-reduced GA [12] with the use of MCTs (M2GA) and of MCTAs (M2GAA). Figure S3 in the Supplemental Material [11] shows the calculated data for the one-stage depth-reduced GA.

The dependencies of the number of gates on the number of qubits have the functional forms used in Sec. III and discussed in Note SI of the Supplemental Material [11]. As one would expect, the numbers of gates for M1GA and M2GA fit well the exponential function of the number of qubits, $G_{M1GA} = 5.0785e^{0.9953n}$ and $G_{M2GA} = 3.8835e^{1.0220n}$, respectively. On the other hand, the power-times-exponential function fits well the number of gates vs the number of qubits for M1GAA and M2GAA, i.e., $G_{M1GAA} = 1.2823n^{2.5439}e^{0.3880n}$ and $G_{M2GAA} = 0.7670n^{2.7057}e^{0.4125n}$. The extrapolations of the fitting functions imply that the M1GA circuit requires over 15 000 000 gates with the 15 qubits and nearly 18 000 000 gates for M2GA. In comparison with 27 000 000 gates for the SGA in Sec. III, the improvement of M1GA and M2GA is significant though it might not be sufficient for practical applications. However, using MCTAs these numbers drastically decrease to about 424 000 and 568 000 for M1GAA and M2GAA, respectively, comparable to 484 000 in the case of the SGA. Thus, one could expect a huge reduction of noise in the circuits using MCTAs, as was already shown in Sec. III for the SGA.

Having in mind the correlation of the number of gates and the selection thresholds for the error probabilities, found in Sec. III, we apply the functional forms used for the number of gates to fit the error thresholds versus the number of qubits for the MGA circuits. Tables SIV and SV in the Supplemental Material [11] show the fitting coefficients in all cases. The calculated data for the selectivity thresholds as well as the fitting curves are shown in Fig. 4 and extrapolated to 15 qubits. Like in the SGA cases of Fig. 2, by setting the threshold of

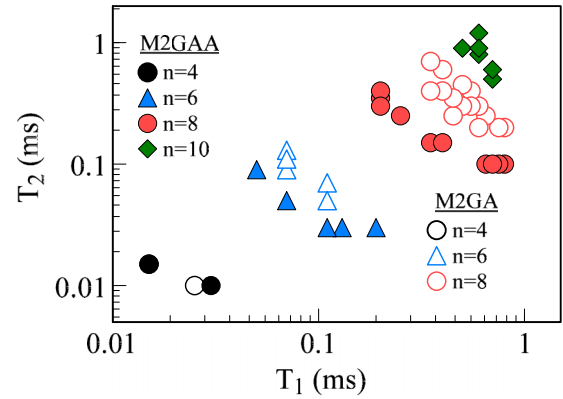


FIG. 5. Selectivity thresholds for thermal noise of two-stage modified Grover's searches [12] (M2GA and M2GAA). Similar results calculated for the one-stage algorithm are shown in Fig. S4 of the Supplemental Material [11].

errors to 10^{-4} it follows that M2GA can perform a successful search with data sets of up to 2^8 in size. Similar results are obtained for M1GA and presented in Fig. S3 of the Supplemental Material [11]. Most error threshold upper bounds are below that limit with a 10-qubit search. However, with the use of MCTAs this data size limit extends to 2^{12} and 2^{14} for M1GAA and M2GAA, respectively.

We also investigate the effect of decoherence by tuning T_1 and T_2 , like in Sec. III. Data points with a selectivity in the range 2.5 to 3.5 are collected and plotted in Fig. 5 for the two-stage depth-reduced method [12]. Similar results for M1GA and M1GAA are calculated and shown in Fig. S4 of the Supplemental Material [11]. The thresholds T_1 and T_2 for 4 qubits are as low as 15 and 15 μs with M2GA, but for 8 qubits with M2GA, the averages of T_1 and T_2 decrease to 500 and 350 μs from 1159 and 330 μs with the SGA. Use of MCTAs helps to further reduce the threshold relaxation times. The coherent requirements for the selectivity with M2GAA yield average values for T_1 and T_2 of 110 and 45 μs , respectively (6 qubits), and 400 and 200 μs for T_1 and T_2 , respectively (8 qubits). For 10 qubits, a successful GA can be achieved by M2GAA with an average of 600 and 800 μs for T_1 and T_2 , respectively, which is about 3 times shorter for T_1 and about 20% for T_2 from the SGAA in Sec. III.

V. COMPARISON AND DISCUSSION OF THE RESULTS

Comparisons of the selectivity thresholds for the error probabilities of the various types of error, obtained with algorithms in Secs. III and IV for 4–10 qubits as well as for the extrapolations to 15 qubits, are presented in Figs. 6(a) (4–8 qubits) and 6(b) (10 and 15 qubits). Due to the presence of quantum noise, the measured probability of the targeted state for a large number of qubits is at a low value. However, the targeted data are still selective and can be distinguished from other data. For example, in the 10-qubit M1GA with depolarizing noise (Fig. S5 of the Supplemental Material [11]), probabilities of the targeted data are about a factor of 2 larger than the highest noise signal, and about 2 orders of magnitude higher than most of the noise signals, which ensures a successful Grover's search. With 4 qubits, SGA,

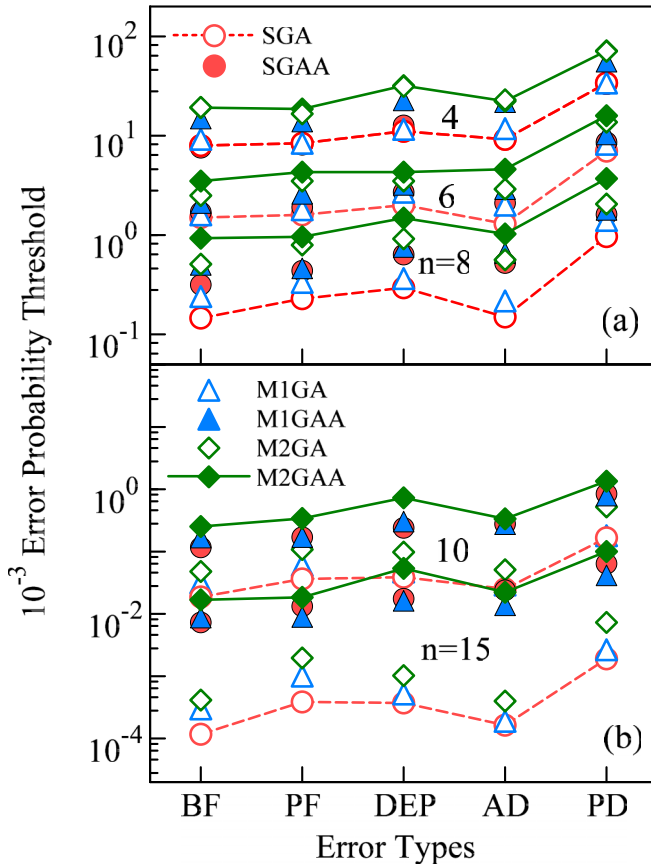


FIG. 6. Comparison of the selectivity thresholds due to various quantum circuits errors in the standard GA (SGA and SGAA when MCTA are used), the one-stage depth-reduced GA (M1GA and M1GAA), and the two-stage depth-reduced GA (M2GA and M2GAA) for (a) 4, 6, and 8 qubits and (b) 10 and 15 qubits. The 15-qubit case was obtained by extrapolation of the fitting curves in Secs. III and IV. Higher-resolution figures are presented in Fig. S6 of the Supplemental Material [11].

SGAA, and M1GA have very similar error thresholds with slightly bigger values of M1GA due to the depth reduction by using local diffusion operators. By applying MCTA in M1GA the selectivity thresholds are increased 1.5 (BF and PF) to 2 times (DEP, AD, and PD). This is not the case for M2GA when $n = 4$, which has similar error threshold values as M2GAA for all types, though slightly bigger than those of M1GAA. However, these relations for the selectivity thresholds are not kept when increasing the number of qubits. Thus, for 10 qubits, the SGAA is significantly more selective than both M1GA (10 times for AD, about 5 times for others) and M2GA and is quite close to the values of M1GAA for all error types. Only M2GAA is convincingly most selective, leading by about a factor of 2 over SGAA and M1GAA except for AD and PD error types where it is only slightly better. The trend of separation of the algorithms which use MCTAs from the algorithms with MCTs is continuing with further increase of the number of qubits by extrapolation of the fitting curves in Secs. III and IV (and Tables SII, SIV, and SV of the Supplemental Material [11]). Thus, with 15 qubits this separation reaches 2 orders of magnitude. In that case, the

M2GA is up to a factor of 2 more selective than M1GA and 2–4 times more selective than the SGA. The trend for relations of M2GAA with M1GAA and SGAA with 15 qubits is similar to that with 10 qubits.

Among all gate errors, depolarization has the highest error threshold in all configurations and is expected to have the least impact to the selectivity of the results in the GA search. Similarly, the phase-damping error thresholds are significantly bigger than those with amplitude damping in all cases. Concerning the considered algorithms, the best results are obtained by two-stage algorithms, whether these are used with MCTs or MCTAs. Moreover, with MCTAs used in the quantum circuits, the decrease in the number of gates with the number of qubits changes from exponential dependence to the product of power and a weak exponential dependence. This leads to a huge improvement in the selectivity loss due to the noise in the circuit, qualifying M2GAA but also SGAA and M1GAA for a successful Grover's search with 10 qubits if error probabilities are smaller than 10^{-4} , i.e., with 15 qubits when the error probabilities are smaller than 10^{-5} .

Therefore, using MCTAs in the quantum circuit in place of MCTs dramatically improves the noise resistance. Using MCTAs in GA is as effective as the use of local diffusion operators in reducing the effect of gate noise, as was done in Ref. [12]. From the discussion in Sec. IV, it follows also that the two-stage MGA contributes the most in the reduction of decoherence.

Nevertheless, the two-stage depth optimization is not supported on current IBM quantum computers because no quantum operations are allowed in the circuits after a measurement (see Fig. S2(c) in Note SII of the Supplemental Material [11]). Another impediment for implementing the optimal configurations is that all simulations in this paper are based on the ideal assumption that all qubits are fully connected to each other, which is not true for the current superconducting quantum computers. Extra SWAP gates could be added to a circuit for adapting to the actual device topology which can dramatically increase the circuit depth after circuit transpiling to basis operations. Other computing platforms could be more successful in handling the quantum noise and thus implementing successfully larger numbers of qubits in Grover's search in the near future. For example, the trapped-ion quantum computers are recognized to have an exceptionally long coherence time, very high fidelity of gate operations, state preparation and readout with a high fidelity, and full connectivity of qubits [26]. Besides, the symmetry features of a trapped-ion device allow for a more compact version of Grover's search with smaller quantum depth [27].

Another drawback in our work could be the way we applied the noise models: These are applied to all qubits in quantum operations in GA. This seems like overestimation of the noise reality. However, this approach could partially compensate for our treatment of the 2-qubit gates (2QGs). It is experimentally known that superconducting 2-qubit gates have significantly higher error probability than 1-qubit gates. In our model an error after a 2QG simply arises from the tensor product of the qubit's states, which is likely underestimating the error of the 2QGs. For example, the number of 2QGs in both the 8-qubit SGA and SGAA circuits is very close to that of

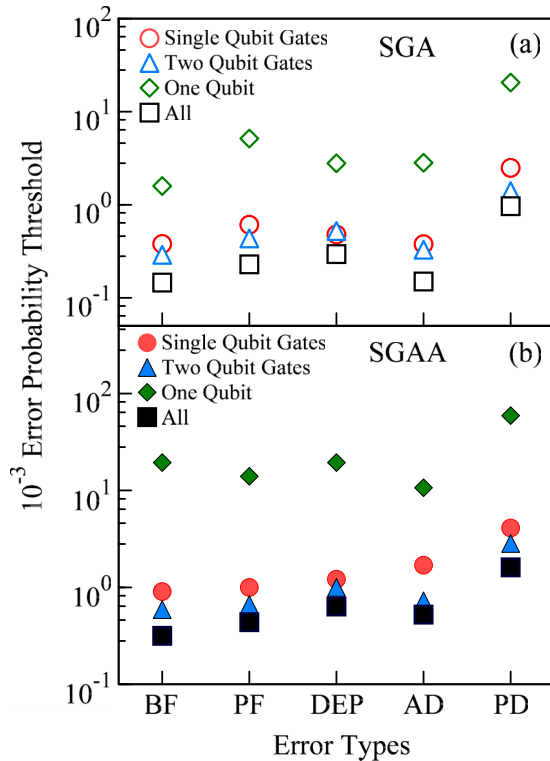


FIG. 7. Error threshold of BF, PF, DEP, AD, and PD with noise channels applied only on single qubit gates and 2-qubit gates for (a) the 8-qubit SGA and (b) the 8-qubit SGAA. Simulated results with only 1 noisy qubit are also shown, as well as contributions of all error channels.

1-qubit gates. We show this by including only noisy 2-qubit gates in the SGA [Fig. 7(a)] and the SGAA [Fig. 7(b)]. We get a slightly lower error threshold than when including only noisy single-qubit gates, indicating that in our model 2-qubit operations contribute only slightly more to a final noise of the GA circuits. Another simplifying assumption is that all qubits are equally susceptible to errors, which is certainly not true in the real superconducting computers. We also test application of noise to only 1 qubit. This gives, in the 8-qubit case for the SGA, an error threshold about an order of magnitude higher (20–60 times for the SGAA) than that for all qubits' GA operations.

VI. CONCLUSIONS

We undertake a series of computer simulations of Grover's search by applying the noise, modeled in the IBM QISKIT. We apply three forms of Grover's algorithm: (i) the standard one, with 4–10 qubits; (ii) a recently published modified Grover's algorithm [12], set to reduce the circuit depth; and (iii) the algorithms in (i) and (ii) with multicontrol Toffoli's gates modified by the addition of an ancilla qubit (MCTAs). The noise and errors included are the bit and phase flips, depolarization, amplitude and phase damping, and the energy and phase relaxation times, determining the system coherence time. The circuits with MCTAs in all cases show a significant improvement of the selectivity thresholds for the error probabilities, which goes up to 1 order of magnitude for a 10-qubit algorithm, and even more for larger numbers of qubits. This is explained by the exponential growth with the number of qubits n when MTAs are used, which transforms into the combination of a power law and weak exponential growth, when MCTAs are utilized. These result in similar functional dependencies on n (with flipped sign of both the exponents and the powers) for the selectivity thresholds due to the errors. The depth-modified Grover's algorithm shows an increase of the error thresholds and a decrease of threshold relaxation times, which are also notably improved by the use of MCTAs. By extrapolation of the fitted functional dependencies to n as large as 15, we also provide predictions of the error thresholds for successful search with all studied quantum circuit configurations, which set the limit for errors probabilities to 10^{-5} for successful search of databases as large as 32 000. While these errors might be beyond anticipated hardware possibilities, the error limit of 10^{-4} seems to be applicable in the near future for a GA search with 10 qubits, i.e., for a data set as large as 1000.

ACKNOWLEDGMENTS

The authors acknowledge financial support from the Institute for Advanced Computational Science at Stony Brook University. We would like to thank Stony Brook Research Computing and Cyberinfrastructure, and the Institute for Advanced Computational Science at Stony Brook University for access to the high-performance SeaWulf computing system, which was made possible by National Science Foundation Grant No. 1531492. The authors are grateful to Kun Zhang and Vladimir Korepin for the inspiring discussions.

- [1] L. K. Grover, Quantum Mechanics Helps in Searching for a Needle in a Haystack, *Phys. Rev. Lett.* **79**, 325 (1997).
- [2] M. Boyer, G. Brassard, P. Høyer, and A. Tapp, Tight bounds on quantum searching, *Fortschr. Phys.* **46**, 493 (1998).
- [3] C. Zalka, Grover's quantum searching algorithm is optimal, *Phys. Rev. A* **60**, 2746 (1999).
- [4] J. Preskill, Quantum computing in the NISQ era and beyond, *Quantum* **2**, 79 (2018).
- [5] D. Reitzner and M. Hillery, Grover search under localized dephasing, *Phys. Rev. A* **99**, 012339 (2019).
- [6] D. D. Bhaktavatsala Rao and K. Mølmer, Effect of qubit losses on Grover's quantum search algorithm, *Phys. Rev. A* **86**, 042321 (2012).
- [7] B. Pablo-Norman and M. Ruiz-Altaba, Noise in Grover's quantum search algorithm, *Phys. Rev. A* **61**, 012301 (1999).
- [8] D. Shapira, S. Mozes, and O. Biham, Effect of unitary noise on Grover's quantum search algorithm, *Phys. Rev. A* **67**, 042301 (2003).
- [9] P. J. Salas, Noise effect on Grover algorithm, *Eur. Phys. J. D* **46**, 365 (2008).

- [10] G. L. Long, Grover algorithm with zero theoretical failure rate, *Phys. Rev. A* **64**, 022307 (2001).
- [11] See Supplemental Material at <http://link.aps.org/supplemental/10.1103/PhysRevA.102.042609> for further details about depth of Grover's algorithm circuit, schematics of the GA quantum circuits, selectivity thresholds for error probabilities and thermal relaxation times for MIGA and MIGAA, examples of 10-qubit MIGA results with depolarizing error, comparison of all tested results and fitting parameters for the selectivity threshold of various types of error.
- [12] K. Zhang and V. E. Korepin, Depth optimization of quantum search algorithms beyond Grover's algorithm, *Phys. Rev. A* **101**, 032346 (2020).
- [13] G. Aleksandrowicz *et al.*, Qiskit: An open-source framework for quantum computing (2019), <https://doi.org/10.5281/zenodo.2562111>.
- [14] A. Barenco, C. H. Bennett, R. Cleve, D. P. DiVincenzo, N. Margolus, P. Shor, T. Sleator, J. A. Smolin, and H. Weinfurter, Elementary gates for quantum computation, *Phys. Rev. A* **52**, 3457 (1995).
- [15] S. S. Tannu and M. K. Qureshi, Not all qubits are created equal: A case for variability-aware policies for NISQ-era quantum computers, in *Proceedings of the Twenty-Fourth International Conference on Architectural Support for Programming Languages and Operating Systems, ASPLOS'19* (Association for Computing Machinery, New York, 2019), pp. 987–999.
- [16] E. Knill, D. Leibfried, R. Reichle, J. Britton, R. B. Blakestad, J. D. Jost, C. Langer, R. Ozeri, S. Seidelin, and D. J. Wineland, Randomized benchmarking of quantum gates, *Phys. Rev. A* **77**, 012307 (2008).
- [17] M. A. Nielsen and I. L. Chuang, *Quantum Computation and Quantum Information*, 10th anniversary ed. (Cambridge University, New York, 2011).
- [18] M. Gutiérrez, L. Svec, A. Vargo, and K. R. Brown, Approximation of realistic errors by Clifford channels and Pauli measurements, *Phys. Rev. A* **87**, 030302(R) (2013).
- [19] J. Preskill, Lecture notes for Ph219/CS219: Quantum information, Chap. 3 (2018), <http://theory.caltech.edu/~preskill/ph229/notes/chap3.pdf>.
- [20] M. Grifoni, E. Paladino, and U. Weiss, Dissipation, decoherence and preparation effects in the spin-boson system, *Eur. Phys. J. B* **10**, 719 (1999).
- [21] Y. Yafet, in *Solid State Physics*, edited by F. Seitz and D. Turnbull (Academic, New York, 1963), p. 2, Vol. 14.
- [22] C. Blank, D. K. Park, J.-K. K. Rhee, and F. Petruccione, Quantum classifier with tailored quantum kernel, *npj Quantum Inf.* **6**, 41 (2020).
- [23] A. Younes, Towards more reliable fixed phase quantum search algorithm, *Appl. Math. Inf. Sci.* **7**, 93 (2013).
- [24] C. Figgatt, D. Maslov, K. A. Landsman, N. M. Linke, S. Debnath, and C. Monroe, Complete 3-qubit Grover search on a programmable quantum computer, *Nat. Commun.* **8**, 1918 (2017).
- [25] High-performance Seawulf computing system, <https://iacs.stonybrook.edu/resources/seawulf-clusters>.
- [26] C. D. Bruzewicz, J. Chiaverini, R. McConnell, and J. M. Sage, Trapped-ion quantum computing: Progress and challenges, *Appl. Phys. Rev.* **6**, 021314 (2019).
- [27] S. S. Ivanov, P. A. Ivanov, I. E. Linington, and N. V. Vitanov, Scalable quantum search using trapped ions, *Phys. Rev. A* **81**, 042328 (2010).